ENGINEERING Information Technology & Electronic Engineering
https://www.academax.com/EITEE; https://www.engineering.org.cn
https://ieeexplore.ieee.org/xpl/RecentIssue.jsp?punumber=11344065
E-mail: eng.itee@zju.edu.cn

Engineering Journals
Available on IEEE Xplore®

Research Article
https://doi.org/10.1631/ENG.ITEE.2025.0110

Design and optimization of a high-efficiency current-biased reverse load modulated power amplifier with impedance and performance constraints

Zhongpeng NI[1], Heng ZHANG[1], Jing XIA[1]✉, Wence ZHANG[1], Wa KONG[1], Chao YU[2], Xiaowei ZHU[2]

[1]*School of Computer Science and Communication Engineering, Jiangsu University, Zhenjiang 212013, China*
[2]*School of Information Science and Engineering, Southeast University, Nanjing 210096, China*

Abstract: We propose an optimization method based on evolutionary computation for the design of broadband high-efficiency current-biased reverse load-modulation power amplifiers (CB-RLM PAs). First, given the reverse load-modulation characteristics of CB-RLM PAs, a comprehensive objective function is proposed that combines multi-state impedance trajectory constraints with in-band performance deviations. For the saturation and 6 dB power back-off (PBO) states, approximately optimal impedance regions on the Smith chart are derived using impedance constraint circles based on load-pull simulations. These regions are used together with in-band performance deviations (e.g., saturated efficiency, 6 dB PBO efficiency, and saturated output power) for matching network optimization and design. Second, a multi-objective evolutionary algorithm based on decomposition with adaptive weights, neighborhood, and global replacement is integrated with harmonic balance simulations to optimize design parameters and evaluate performance. Finally, to validate the proposed method, a broadband CB-RLM PA operating from 0.6 to 1.8 GHz is designed and fabricated. Measurement results show that the efficiencies at saturation, 6 dB PBO, and 8 dB PBO all exceed 43.6%, with saturated output power being maintained at 40.9–41.5 dBm, which confirms the feasibility and effectiveness of the proposed broadband high-efficiency CB-RLM PA optimization and design approach.

Key words: Current-biased reverse load-modulation; Broadband; High efficiency; Power amplifier; Optimization

1 Introduction

With the modern communication systems advancing toward higher data rates and broader coverage, the peak-to-average power ratio (PAPR) of modulated signals increases significantly (Iqbal et al., 2025). This trend imposes more stringent requirements on the design of power amplifiers (PAs) with high efficiency at a larger power back-off (PBO) (Zhou et al., 2022; Giofrè et al., 2024; Zhang Y et al., 2025b). So, the Doherty power amplifier (DPA) has attracted wide attention because its circuit is relatively simple and it maintains high efficiency and linearity at PBO. However, conventional DPAs typically rely on a quarter-wavelength ($\lambda/4$) impedance transformer to realize the required load modulation; the dispersive characteristic of this element severely limits the effective operating bandwidth in broadband operation (Doherty, 1936; Akbarpour et al., 2012).

To extend the bandwidth, various improvements have been proposed, such as reactance compensation (Xia et al., 2016; Yang et al., 2019; Xiao F et al., 2021), modified load-modulation structures (Pang et al., 2015; Zhou et al., 2017), and reciprocal bias configurations (Gao et al., 2022; Zhang Y et al., 2025a). Although these methods expand the operating band to some extent, they remain fundamentally constrained by the $\lambda/4$ transformer architecture, which makes it difficult to achieve a large fractional bandwidth while ensuring high efficiency. To address the aforementioned issues, Akbarpour et al. (2017) proposed a novel power amplifier architecture using a constant current source at the drain for direct current (DC) biasing. By exploiting the reverse load-modulation behavior of current-biased transistors, the operating band at PBO can be effectively expanded without a conventional $\lambda/4$ impedance transformer. Therefore, this architecture is a promising approach to broadband high-efficiency PA design. However, owing to the intrinsic characteristics of

✉ Jing XIA, jingxia@ujs.edu.cn
Jing XIA, https://orcid.org/0000-0001-6255-9297
CLC number: TN722

Received: Oct. 31, 2025; Revision accepted: Jan. 14, 2026;
Crosschecked: Jan. 16, 2026

transistors and the reverse load-modulation mechanism, it remains difficult to match impedances that meet high-efficiency requirements across different operating states over a wide band.

Given its excellent global search capabilities, evolutionary computation has been widely used in radio frequency (RF) design and automated optimization (Zhang H et al., 2024; Fan et al., 2025; Hong et al., 2025; Jin et al., 2025; Ni et al., 2025b, 2025c). Chen et al. (2020) used the multi-objective evolutionary algorithm based on decomposition (MOEA/D) to optimize output power, efficiency, and gain for a high-efficiency DPA at 3.5 GHz. In Kong et al. (2024), MOEA/D was applied to optimize the output matching network (OMN) impedances for different operating states. Although these studies have made progress, the constant current-biased reverse load-modulation power amplifier (CB-RLM PA) has a unique load-modulation mechanism, and how to apply this methodology effectively to CB-RLM PA design remains to be further explored.

Therefore, to address the load-modulation characteristics and efficiency enhancement requirements of the CB-RLM PA under wideband conditions, this paper proposes a design framework that combines multi-state impedance trajectory constraints with performance optimization. First, the OMN impedance trajectory is constrained by matching in two states (saturation and PBO). Next, harmonic balance (HB) simulation is used to evaluate output power and efficiency, and the matching network is optimized to obtain balanced performance across operating states. To validate the approach, MOEA/D with adaptive weights, neighborhood adaptation, and global replacement (MOEA/D-ANGR) is employed for optimization (Ni et al., 2025a). The designed PA achieves a saturated output power (P_{SAT}) above 40.9 dBm over 0.6–1.8 GHz and a drain efficiency (DE) above 43.6% at saturation, 6 dB PBO, and 8 dB PBO. These results demonstrate the effectiveness of the method.

2 Theoretical analysis

2.1 Current-biased reverse load-modulation power amplifier

Conventional PAs typically use constant voltage sources at the gate and drain for DC biasing, as shown in Fig. 1a. Under dynamic load conditions, the output power of a transistor under voltage bias increases as the load impedance decreases, indicating a negative correlation, as shown in Fig. 1b. This load-modulation behavior is contrary to the objective of active load-modulation. Consequently, in a conventional DPA, a $\lambda/4$ transformer is inserted in the carrier path so that the carrier amplifier reaches saturation earlier, thereby improving efficiency at PBO (Moreno Rubio et al., 2018; Zhang ZW et al., 2022; Sun et al., 2023). On the contrary, a high-efficiency PA architecture that biases the transistor with a constant current source was proposed in Akbarpour et al. (2017). The basic structure is demonstrated in Fig. 2a. In this architecture, the drain is biased by a constant current source. Compared with a transistor under voltage bias, a transistor under current source bias exhibits fundamentally different load-modulation behavior. Specifically, its output power increases with increasing load impedance, showing a positive correlation, as illustrated in Fig. 2b. This characteristic is the opposite of the conventional voltage-biased structure. Therefore, if the load-modulation under voltage bias is termed forward load-modulation, the behavior under current source bias can be regarded as reverse load-modulation. Thus, the CB-RLM PA does not rely on a $\lambda/4$ impedance transformer to realize load-modulation in the PBO region. Instead, a lower equivalent load impedance is presented to the carrier branch at PBO so that the carrier PA can enter the high-efficiency operating region at a lower output power. As the peaking branch gradually turns on, the equivalent load impedance of the carrier PA is continuously modulated and can smoothly transition from a normalized value of approximately 0.5 to a normalized value of 1 as shown in Fig. 2c.

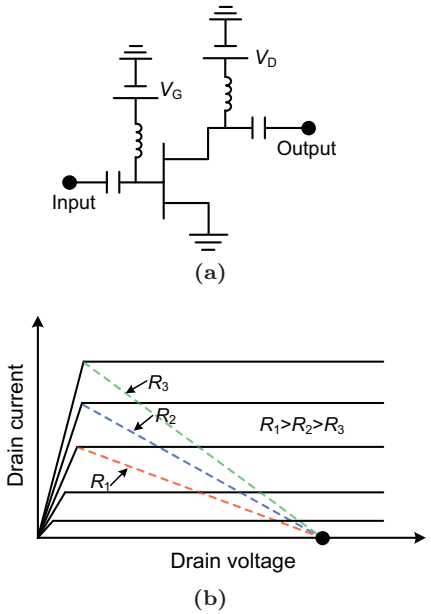

Fig. 1 Transistor biased by voltage: (a) circuit schematic; (b) load line

Fig. 3 illustrates the basic architecture of the CB-RLM PA. Unlike a conventional DPA, this scheme introduces a constant current source at the drain of the carrier branch, thereby altering the load-modulation behavior and extending the operating bandwidth. The PBO range is defined as the ratio of the output power at saturation to that at power back-off (Zhao et al., 2021). Under a symmetric design (i.e., the saturation power ratio between the peaking and carrier amplifiers is $\alpha = 1$), the PBO range can be derived from the equivalent reflection coefficient Γ based on Fang and Cheng (2014), as follows:

$$\begin{aligned}\mathrm{PBO}_{\mathrm{range}} &= 10\lg\left(\frac{P_{\mathrm{SAT}}}{P_{\mathrm{PBO}}}\right)\\ &= 10\lg\left[(1+\alpha)\frac{1+|\Gamma|}{1-|\Gamma|}\right]\\ &= 10\lg\left(\frac{2(1+|\Gamma|)}{1-|\Gamma|}\right),\end{aligned} \tag{1}$$

where P_{SAT} and P_{PBO} denote the output power at saturation and at PBO, respectively. The coefficient Γ is determined by the equivalent output impedances of the carrier branch at these operating states, namely $Z_{\mathrm{C,SAT}}$ and $Z_{\mathrm{C,PBO}}$.

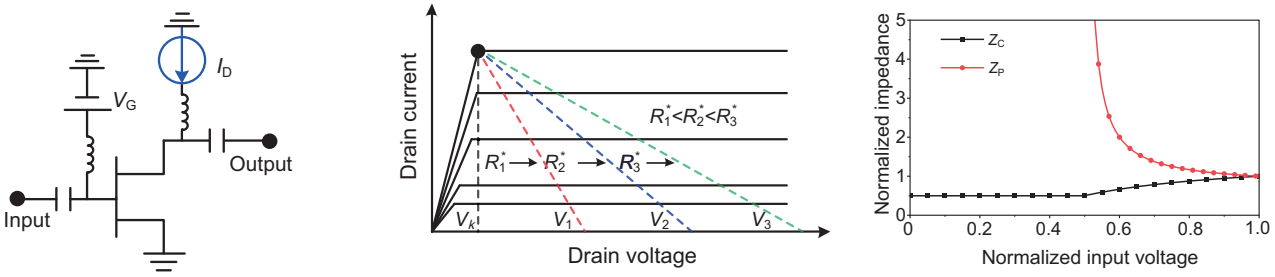

Fig. 2 Transistor biased by current: (a) circuit schematic; (b) load line; (c) load impedance and input voltage

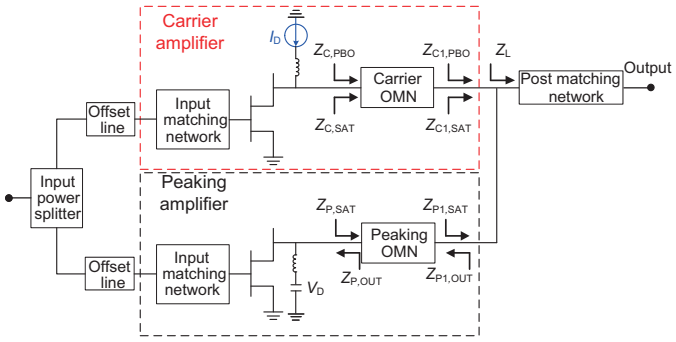

Fig. 3 Schematic of the current-biased reverse load-modulation power amplifier

$$|\Gamma| = \left| \frac{Z_{\mathrm{C,SAT}} - Z_{\mathrm{C,PBO}}}{Z_{\mathrm{C,SAT}} + Z_{\mathrm{C,PBO}}} \right|. \tag{2}$$

Note that in practical designs, the equivalent output impedance of the carrier branch at PBO, $Z_{\mathrm{C,PBO}}$, is often not purely resistive. It is influenced by the equivalent impedance Z_{L} of the post-matching network (PMN) and by the peaking branch output impedance $Z_{\mathrm{P,OUT}}$. Previous studies have shown that jointly optimizing Z_{L} and $Z_{\mathrm{P,OUT}}$ can effectively extend the PBO range (Fang and Cheng, 2014; Li et al., 2020; Xiao ZH et al., 2023). Furthermore, existing designs indicate that this PA architecture involves multiple interdependent factors, and that the design process is hindered by numerical difficulties and reliance on designer experience. Therefore, based on the load-modulation mechanism under current source bias, we propose a simple CB-RLM PA design method.

2.2 Proposed objective function

To achieve high efficiency across operating states, load-modulated PAs must dynamically adjust the load impedance. Therefore, we incorporate an impedance constraint into the optimization to ensure that the matching network impedance trajectory remains within a desired impedance region. Because the optimal impedance region obtained from load-pull simulations typically has a complex, irregular shape, it is difficult to describe with analytical expressions. Accordingly, the impedance constraint circle method described in Kong et al. (2024) is adopted. Specifically, as shown in Fig. 4, an impedance constraint circle is constructed on the Smith chart, centered at the target impedance Z_{c} with radius r_{g}. This circle defines the allowable deviation for the matching network

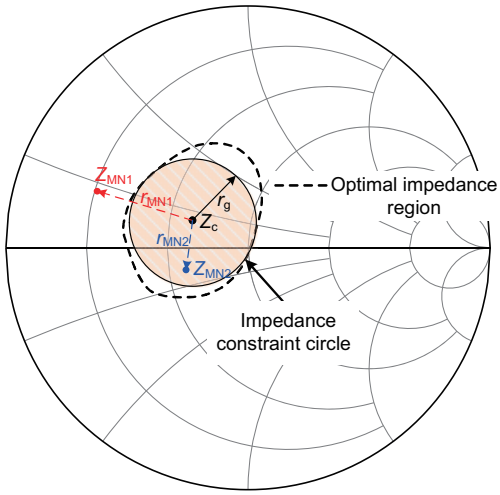

Fig. 4 Impedance constraint circle on the Smith chart

output impedance.

During optimization, the distance between the impedance obtained by the matching network Z_{MN} and the target impedance Z_{center} is defined as follows:

$$y_{\mathrm{r}} = \left| \frac{Z_{\mathrm{MN}} - Z_{\mathrm{center}}}{Z_{\mathrm{MN}} + \mathrm{conj}(Z_{\mathrm{center}})} \right|. \tag{3}$$

The impedance error at different frequencies f is further defined as

$$E_{\mathrm{r}}(f) = \max\left(0, (y_{\mathrm{r},f} - r_{\mathrm{g},f})\right). \tag{4}$$

Thus, the impedance constraint function F_1 can be obtained:

$$F_1 = \sum_{f \in B} \max(E_{\mathrm{r,PBO}}(f), E_{\mathrm{r,SAT}}(f)), \tag{5}$$

where B denotes the set of discrete frequencies within the operating band. If $F_1 = 0$, then all design frequencies in the band satisfy the impedance constraints in both the saturation and PBO states.

To simultaneously expand bandwidth and enhance efficiency, the carrier OMN ($\mathrm{OMN_c}$), the peaking OMN ($\mathrm{OMN_p}$), and the PMN in a CB-RLM PA must be designed to provide appropriate impedance matching across operating states. However, accurate analytical solutions are often difficult to obtain for broadband operation. Therefore, to evaluate the performance of the CB-RLM PA, we define in-band normalized performance error functions for efficiency and output power

under the two critical and commonly used operating states in load-modulated PA design, namely saturation and PBO. The in-band errors are defined as follows, where the desired performance targets are $\mathrm{DE}_{\mathrm{PBO}}$, $\mathrm{DE}_{\mathrm{SAT}}$, and P_{SAT}, respectively:

$$E_{\mathrm{DE,PBO}} = \max\left(0, \frac{\mathrm{DE}_{\mathrm{PBO}} - \min_{f\in B}(y_{\mathrm{DE}_{\mathrm{PBO}}})}{\mathrm{DE}_{\mathrm{PBO}}}\right), \tag{6}$$

$$E_{\mathrm{DE,SAT}} = \max\left(0, \frac{\mathrm{DE}_{\mathrm{SAT}} - \min_{f\in B}(y_{\mathrm{DE}_{\mathrm{SAT}}})}{\mathrm{DE}_{\mathrm{SAT}}})\right), \tag{7}$$

$$E_{P_{\mathrm{out}}} = \max\left(0, \frac{P_{\mathrm{SAT}} - \min_{f\in B}(y_{P_{\mathrm{SAT}}})}{P_{\mathrm{SAT}}}\right), \tag{8}$$

where $y_{\mathrm{DE}_{\mathrm{PBO}}}$, $y_{\mathrm{DE}_{\mathrm{SAT}}}$, and $y_{P_{\mathrm{SAT}}}$ denote the performance of the CB-RLM PA at the corresponding state and frequency.

The above three performance metrics constitute the performance objective F_2. When all the frequencies to be designed in the band meet the specified efficiency and power requirements, $F_2 = 0$.

$$F_2 = E_{\mathrm{DE,PBO}} + E_{\mathrm{DE,SAT}} + E_{P_{\mathrm{out}}}. \tag{9}$$

2.3 Multi-objective optimization problem

In PA design, it is usually necessary to make trade-offs among multiple objectives such as load impedance and in-band performance. This problem can be formulated as a multi-objective optimization problem:

$$\min_{\boldsymbol{x}\in X} \boldsymbol{F}(\boldsymbol{x}) = \left(\boldsymbol{F}_1(\boldsymbol{x}), \boldsymbol{F}_2(\boldsymbol{x}), \ldots, \boldsymbol{F}_M(\boldsymbol{x})\right), \tag{10}$$

where $\boldsymbol{x}$ denotes the vector of design variables (e.g., microstrip lengths and widths), X represents the feasible solution space, and $\boldsymbol{F}(\boldsymbol{x})$ is the vector of M objective functions.

MOEA/D decomposes a multi-objective optimization problem into a set of scalar subproblems, which evolve jointly to approximate the Pareto front (PF). However, the original MOEA/D typically relies on uniform weights and fixed neighborhoods. When the PF has discontinuities or long tails, uniform weights hinder balanced coverage, and fixed neighborhoods cause the search to become overly localized in the later stages of evolution. In addition, traditional methods often select parents within the neighborhood and prioritize their offspring when updating subproblems, which is inefficient when offspring directions misalign with neighborhood weights. To address these issues, Ni et al. (2025a) proposed MOEA/D-ANGR, which adaptively adjusted the densities and positions of weight vectors during distribution and search to enhance the coverage of complex PFs. It also adapted the neighborhood size according to the position of a weight vector on the reference hyperplane and the stage of evolution, enabling a smooth transition from broad exploration early on to local refinement later. Furthermore, it used information from high-quality offspring to update the entire population, which improved the global optimization efficiency. Given the high dimensionality and complex constraints of CB-RLM PA optimization, we employ MOEA/D-ANGR to optimize the impedance trajectory under multiple states for the matching network and the PA performance within the operating band.

3 Design of broadband high-efficiency reverse load-modulation PA

To validate the proposed design method, a CB-RLM PA was designed using MACOM CGH40006P GaN transistors operating from 0.6 to 1.8 GHz. The circuit was fabricated on a Taconic TLY-5 substrate with a dielectric constant of 2.2 and a thickness of 20 mil. The carrier amplifier used a constant current source for the drain bias set to 460 mA and a gate bias of −1.6 V. The peaking amplifier used a 28 V drain bias and a gate bias of −6 V.

Fig. 5 shows the schematic of the CB-RLM PA to be optimized. The architecture consists of a power divider, two phase offset lines, a class AB carrier PA biased by a constant current source, a class C peaking PA biased by voltage, and a PMN. To simplify the overall design and optimization, the input matching network (IMN) was designed before the optimization to satisfy the source impedance requirements under two different bias conditions. The proposed CB-RLM PA design process is as follows.

Based on the analysis in Section 2.2, fundamental load-pull simulations were performed for the current-biased carrier amplifier at 0.6, 1.2, and 1.8 GHz under two operating states (saturation and PBO) to ensure effective load-modulation. To obtain a more accurate desired impedance region, the

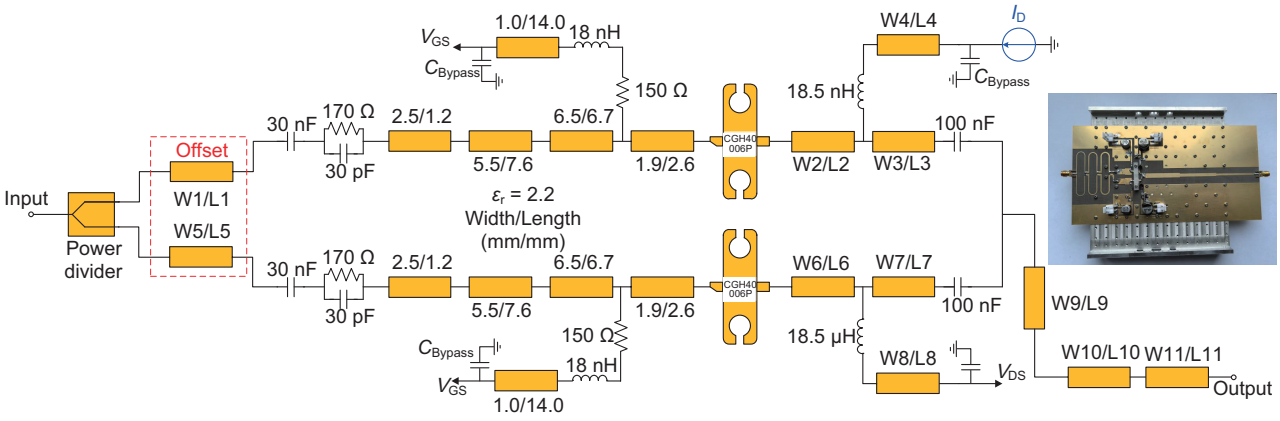

Fig. 5 Schematic of the current-biased reverse load-modulation power amplifier to be optimized

fundamental and harmonic load-pull simulations were carried out iteratively. The extracted harmonic load impedances were then used as fixed terminations for subsequent fundamental load-pull simulations. The design requires DE $\geq$ 45% at saturation and at PBO. Accordingly, the impedance constraint circle method was used to obtain the desired impedance regions. Fig. 6 details the optimal impedance regions and the corresponding target regions at the design frequencies.

Second, considering that PAs must maintain high efficiency across different PBO ranges in practical applications, it was required that DE $\geq$ 45% in both the saturation and PBO states, with $P_{\mathrm{SAT}} \geq 40.8$ dBm. The optimization covered seven frequencies from 0.6 to 1.8 GHz (0.6, 0.8, 1.0, 1.2, 1.4, 1.6, and 1.8 GHz). The ranges of the design variables are listed in Table 1. Because W1 and W5 were the width parameters of the phase offset line, they were fixed at a 50 Ω microstrip (approximately 1.5 mm).

Next, MOEA/D-ANGR from Ni et al. (2025a) was employed in conjunction with HB simulation for optimization, with a population size of 100 for 50 iterations. The detailed process is shown in Fig. 7. Specifically, the electromagnetic simulation software received the design parameters from the optimization algorithm, automatically constructed the circuit, and performed HB simulation. After each simulation, the load impedances, efficiencies, and output powers for different operating states were returned to the optimization algorithm to compute the objective functions and update the population. The algorithm was then iterated until the termination criteria were met.

Fig. 8 shows the convergence curve of the proposed method during the optimization process, i.e., the change in the optimal objective function value (the minimum of the sum of the two objectives) for each generation as a function of the iteration count. The figure shows that this value decreased rapidly at the beginning and approached zero by generation 24, which indicated that the OMN and PMN parameters met the

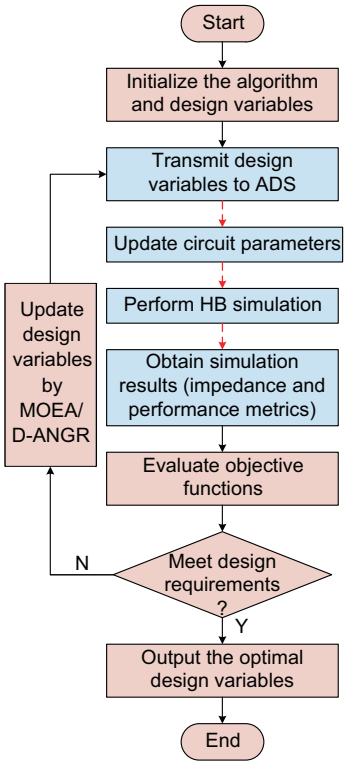

Fig. 7 Flowchart of the proposed method

design requirements. Fig. 9 depicts the impedance trajectories at different iterations. The impedance trajectory of the initial design was far from the desired regions, while that of the 10$^{\mathrm{th}}$ generation partially entered and adjusted toward the desired direction. The impedance trajectory of the final generation fell within the target impedance region at the three frequencies of 0.6, 1.2, and 1.8 GHz, indicating that the carrier OMN has achieved the required dual-state matching. Fig. 10 shows that, as the iteration progressed, the performance indicators of the CB-RLM PA, such as efficiency and output power, were

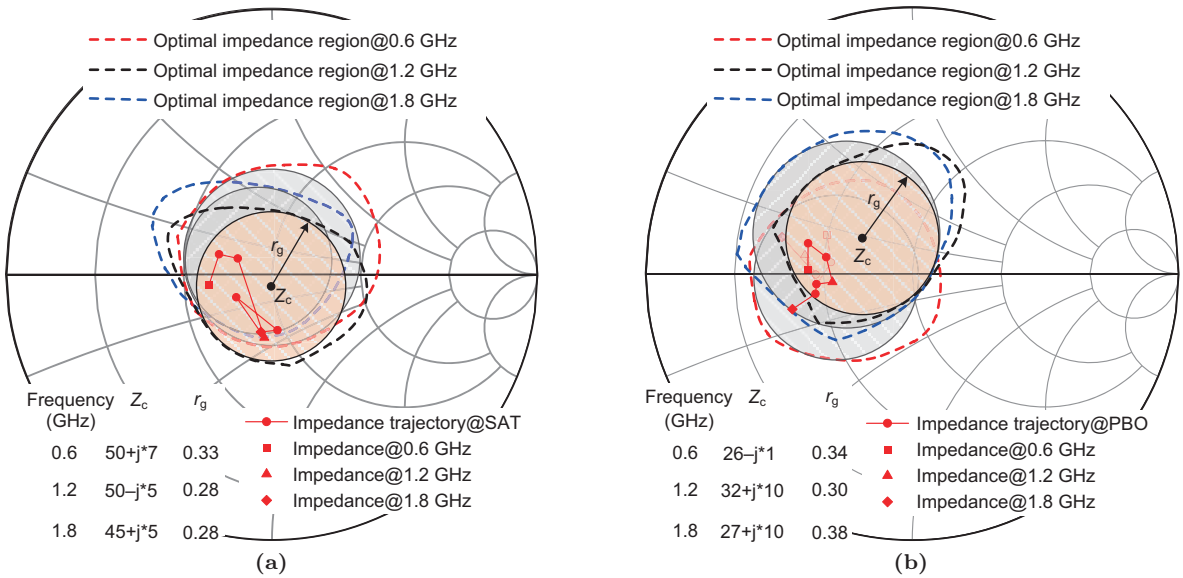

Fig. 6 Desired impedance regions and OMN impedance trajectories for different states: (a) SAT; (b) PBO

Table 1 Design variables and parameters (in mm)

	W1	W2	W3	W4	W5	W6	W7	W8	W9	W10	W11
LB	1.5	1.4	1.0	1.0	1.5	1.4	1.0	1.0	1.0	1.0	1.0
UB	1.5	5.0	5.0	3.0	1.5	5.0	5.0	3.0	5.0	5.0	5.0
Gen 0	1.5	4.6	2.6	2.1	1.5	1.7	2.4	1.7	3.4	2.2	4.1
Gen 10	1.5	4.9	2.5	1.8	1.5	2.9	2.3	2.0	4.0	3.9	2.1
Gen 50	1.5	2.0	5.0	1.1	1.5	2.9	4.8	1.5	4.3	3.3	2.0
	L1	L2	L3	L4	L5	L6	L7	L8	L9	L10	L11
LB	1.0	0.3	0.3	2.0	1.0	0.3	0.3	2.0	30.0	30.0	30.0
UB	10.0	5.0	5.0	10.0	10.0	5.0	5.0	10.0	50.0	50.0	50.0
Gen 0	7.3	3.1	2.3	9.4	6.4	4.8	3.2	5.0	45.0	34.6	42.5
Gen 10	9.2	3.8	1.5	7.6	3.7	3.9	1.8	2.7	32.2	31.2	32.9
Gen 50	3.0	0.8	0.9	5.5	7.2	2.2	1.0	6.7	39.2	37.3	41.4

LB: lower bound; UB: upper bound

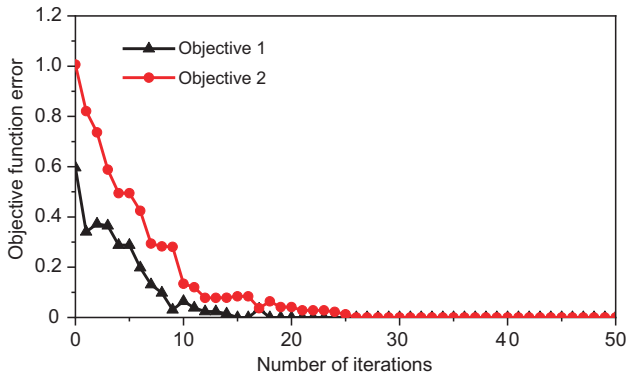

Fig. 8 Objective function error versus the number of iterations

gradually improved and met the design requirements. Fig. 11 details the curves of efficiency and gain versus output power for the designed CB-RLM PA. Within the entire operating band, the saturated out put power remained within 41.2–42.0 dBm, and the saturated and 8 dB PBO DEs were maintained at 53.7%–68.6% and 45.6%–51.5%, respectively. At 6 dB PBO, the DE ranged from 45.6% to 53.8%, which demonstrated excellent broadband performance. Fig. 12 shows the trajectories of the impedances at the package plane for the carrier and peaking PAs versus input power. It can be observed that, by imposing impedance constraints at both saturation and PBO states, the designed PA satisfied the required load-modulation behavior as the input power level varied.

4 Manufacturing and measurement

To validate the proposed design method, a 0.6–1.8 GHz broadband CB-RLM PA was fabricated and measured. The prototype is as shown in Fig. 5. First, a continuous-wave signal with spacing of 200 MHz was used to analyze the performances of the designed CB-RLM PA across the entire bandwidth. The measurement results are shown in Figs. 13 and 14. It can be seen from the figures that the fabricated CB-RLM PA achieved an output power of 40.9–41.5 dBm and a DE of 53.2%–63.9% at saturation. Meanwhile, its 8 dB and 6 dB PBO DEs remained in the ranges of 43.6%–53.2% and 45.4%–58.7%, respectively. The measurement results were consistent with the simulation results, which validated the feasibility of the theoretical analysis and the design methodology.

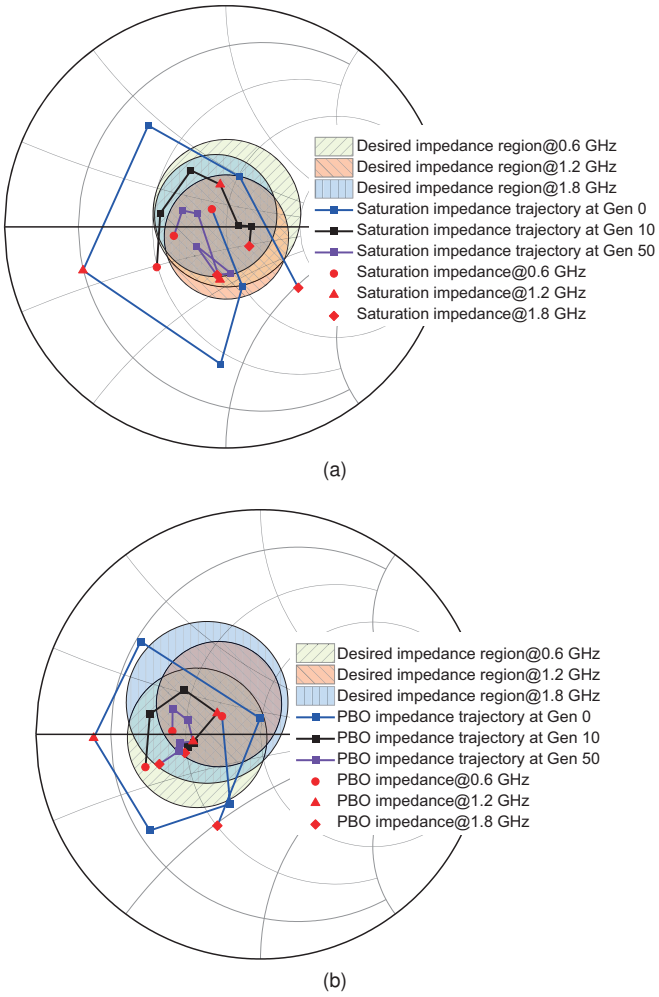

Fig. 9 Carrier OMN impedance trajectories at different generations: (a) SAT; (b) PBO

Second, digital predistortion (DPD) was applied at frequencies of 0.6, 1.2, and 1.8 GHz. Fig. 15 shows the normalized power spectral density (PSD) with and without DPD. With DPD enabled, the in-band adjacent-channel leakage ratio (ACLR) was below −45.5 dBc. Table 2 compares the proposed PA with recently reported broadband load-modulated PAs. The results showed that the proposed CB-RLM PA achieved favorable bandwidth and efficiency at 6 dB and 8 dB PBO, further confirming the effectiveness of the method.

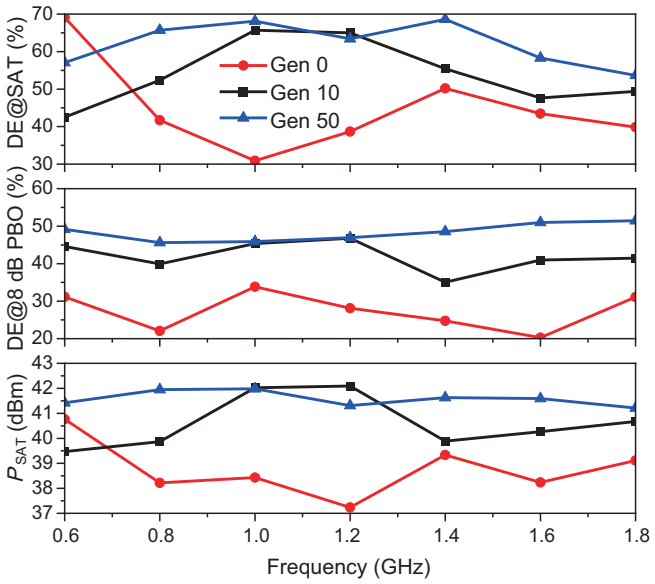

Fig. 10 Performance metrics at different generations

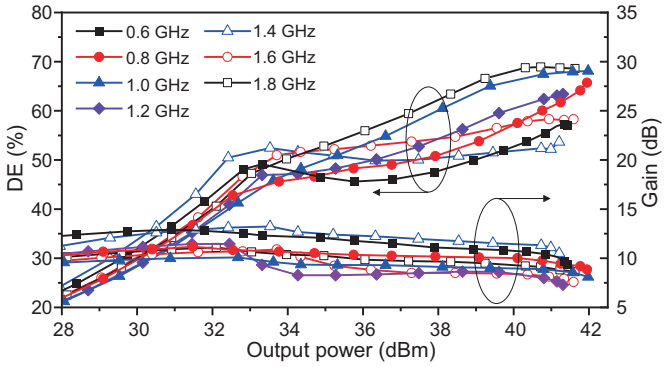

Fig. 11 Simulated efficiency and gain versus output power at various frequencies

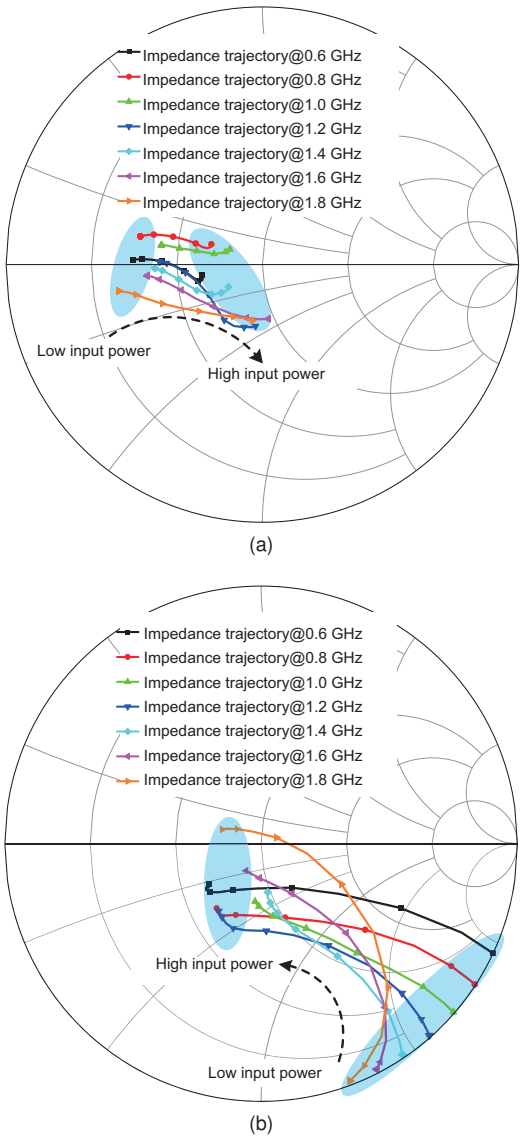

Fig. 12 Load-modulation trajectories: (a) carrier; (b) peaking

5 Conclusions

We propose a CB-RLM PA design method that jointly enforces multi-state impedance trajectory constraints and optimizes in-band performance. The approach considers both impedance modulation behavior and performance metrics, and uses MOEA/D-ANGR to optimize the CB-RLM PA across different operating states. Across the entire band, the fabricated PA achieved a saturated output power of 40.9–41.5 dBm. The saturated efficiency and the efficiency at 8 dB PBO were 53.2%–63.9% and 43.6%–53.2%, respectively. At 6 dB PBO, the efficiency remained between 45.4% and 58.7%, demonstrating strong broadband performance and robustness at PBO.

Acknowledgments

This work was supported by the National Natural Science Foundation of China (Nos. 62171204, 62171129, and 62001192).

Author contributions

Zhongpeng NI designed the research. Heng ZHANG and Jing XIA processed the data. Zhongpeng NI, Wence ZHANG, and Wa KONG drafted the paper. Chao YU and Xiaowei ZHU helped organize the paper. Zhongpeng NI and Jing XIA revised and finalized the paper.

Table 2 Performance comparison with published PAs

Reference	Frequency (GHz)	FBW (%)	P_{SAT} (dBm)	Gain (dB)	DE@SAT (%)	DE@6 dB (%)	DE@8 dB (%)
Akbarpour et al. (2017)	0.8–2.2	93.3	39.7–40.7	7.9–8.9*	46.0–64.0	38.0–45.0*	36.9–47.0*
Gan et al. (2020)	1.7–2.6	41.9	43.2–45.2	9.1–11.2	58.4–69.1	46.3–57.7	39.8–53.0*
Liu et al. (2020)	1.4–2.55	58.2	41.9–42.2	9.1–12.2*	62.0–74.0	48.0–58.0	39.0–61.0*
Fang et al. (2024)	1.0–3.0	100.0	36.5–38.7	6.3–8.8*	47.8–57.7	45.4–51.2	38.8–48.9*
Zhang H et al. (2025)	1.2–2.8	80.0	43.1–44.5	7.1–8.9	54.1–74.2	50.9–56.5	42.5–47.2*
Ju et al. (2025)	2.8–4.2	40.0	42.2–43.1	7.0–8.4	51.0–61.0	43.0–53.8*	43.0–50.8
This paper	0.6–1.8	100.0	40.9–41.5	7.2–10.5	53.2–63.9	45.4–58.7	43.6–53.2

*Values estimated from the corresponding figures (not reported in tables)

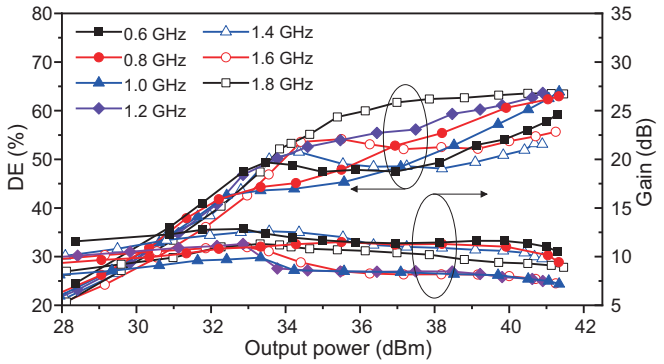

Fig. 13 Measured efficiency and gain versus output power

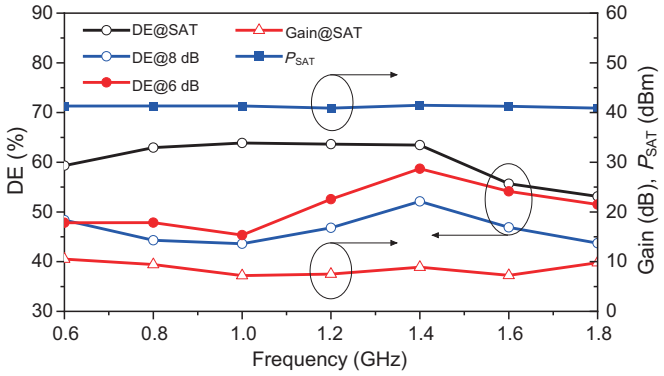

Fig. 14 Measured performance metrics at different frequencies

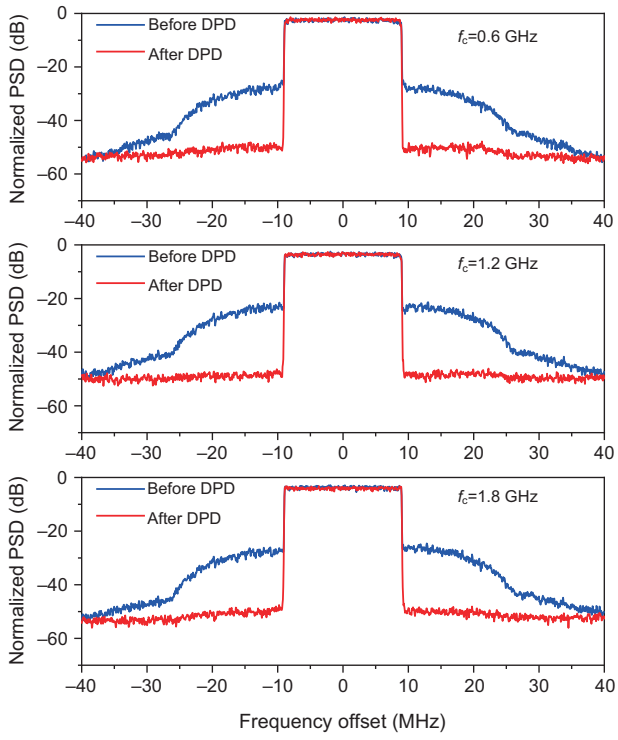

Fig. 15 Measured spectra with and without DPD at three frequencies

Conflict of interest

All the authors declare that they have no conflict of interest.

Data availability

The data that support the findings of this study are available from the corresponding author upon reasonable request.

Declaration on the use of generative AI tools

During the preparation of this work, the authors used ChatGPT to improve language. After using this tool, the authors reviewed and edited the content as needed and take full responsibility for the content of the published article.

References

Akbarpour M, Helaoui M, Ghannouchi FM, 2012. A transformer-less load-modulated (TLLM) architecture for efficient wideband power amplifiers. *IEEE Trans Microw Theory Tech*, 60(9):2863-2874. https://doi.org/10.1109/TMTT.2012.2206050

Akbarpour M, Ghannouchi FM, Helaoui M, 2017. Current-biasing of power-amplifier transistors and its application for ultra-wideband high efficiency at power back-off. *IEEE Trans Microw Theory Tech*, 65(4):1257-1271. https://doi.org/10.1109/TMTT.2016.2645149

Chen CH, Yang YS, Chen CY, et al., 2020. Circuit-simulation-based design optimization of 3.5 GHz Doherty power amplifier via multi-objective evolutionary algorithm and unified optimization framework. IEEE Int Symp on Radio-Frequency Integration Technology, p.76-78. https://doi.org/10.1109/RFIT49453.2020.9226245

Doherty W, 1936. A new high efficiency power amplifier for modulated waves. *Proc Inst Radio Eng*, 24(9):1163-1182. https://doi.org/10.1109/JRPROC.1936.228468

Fan Z, Hao Z, Jin B, et al., 2025. Design of RF PAs using PSO algorithm with dynamic nonlinear self-adaptive hyperparameters. *IEEE Trans Microw Theory Tech*, 73(4):2157-2169. https://doi.org/10.1109/TMTT.2024.3520173

Fang X, Cheng KKM, 2014. Extension of high-efficiency range of Doherty amplifier by using complex combining load. *IEEE Trans Microw Theory Tech*, 62(9):2038-2047. https://doi.org/10.1109/TMTT.2014.2333713

Fang X, Chen R, Shi J, 2024. Switchless class-G power amplifiers: generic theory and design methodology using packaged transistors. *IEEE Trans Microw Theory Tech*, 72(8):4625-4637. https://doi.org/10.1109/TMTT.2024.3351852

Gan DC, Shi WM, He SB, et al., 2020. Broadband Doherty power amplifier with transferable continuous mode. *IEEE Access*, 8:99485-99494. https://doi.org/10.1109/ACCESS.2020.2997826

Gao RB, Pang JZ, Cai TF, et al., 2022. Dual-band three-way Doherty power amplifier employing dual-mode gate bias and load compensation network. *IEEE Trans Microw Theory Tech*, 70(4):2328-2340. https://doi.org/10.1109/TMTT.2022.3149379

Giofrè R, Piacibello A, Camarchia V, et al., 2024. A two-way GaN Doherty amplifier for 5G FR2 with extended back-off range. *IEEE Microw Wirel Technol Lett*, 34(3):314-317. https://doi.org/10.1109/LMWT.2024.3350435

Hong YG, Huang JJ, Cai JL, 2025. Design of broadband RF PAs using an improved Bayesian optimization algorithm. *IEEE Trans Microw Theory Tech*, 73(10):7469-7481. https://doi.org/10.1109/TMTT.2025.3566709

Iqbal M, Peppas I, Pitton M, et al., 2025. An integrated Doherty power amplifier module based on an advanced GaN-on-Si HEMT technology and a wideband power combiner. *IEEE Microw Wirel Technol Lett*, 35(6):828-831. https://doi.org/10.1109/LMWT.2025.3567969

Jin BH, Crupi G, Cai JL, 2025. Design of multi-octave RF PA based on PSO method with individually self-adaptive hyperparameters. Int Workshop on Integrated Nonlinear Microwave and Millimetre-Wave Circuits, p.1-3. https://doi.org/10.1109/INMMIC64198.2025.10975563

Ju Y, Chen Y, Bae S, et al., 2025. Load network for broadband Doherty power amplifiers using non-foster characteristics of a coupled transmission line. *IEEE Trans Microw Theory Tech*, 73(11):8845-8856. https://doi.org/10.1109/TMTT.2025.3596926

Kong W, Zhong Y, Xia J, et al., 2024. Optimization design of broadband Doherty PA using fragment-type matching network based on dual-state impedance objective function. *IEEE Trans Circ Syst II Expr Briefs*, 71(4):1809-1813. https://doi.org/10.1109/TCSII.2023.3332178

Li C, You F, Peng J, et al., 2020. Co-design of matching sub-networks to realize broadband symmetrical Doherty with configurable back-off region. *IEEE Trans Circ Syst II Expr Briefs*, 67(10):1730-1734. https://doi.org/10.1109/TCSII.2019.2946395

Liu HY, Fang XH, Cheng KKM, 2020. Bandwidth enhancement of frequency dispersive Doherty power amplifier. *IEEE Microw Wirel Compon Lett*, 30(2):185-188. https://doi.org/10.1109/LMWC.2019.2963542

Moreno Rubio JJ, Camarchia V, Pirola M, et al., 2018. Design of an 87% fractional bandwidth Doherty power amplifier supported by a simplified bandwidth estimation method. *IEEE Trans Microw Theory Tech*, 66(3):1319-1327. https://doi.org/10.1109/TMTT.2017.2767586

Ni ZP, Xia J, Zhou XY, et al., 2025a. Design and analysis of optimization method for ultra-wideband PA based on improved MOEA/D algorithm using mixed objective function. *IEEE Trans Comput Aided Des Integr Circ Syst*, 44(7):2641-2654. https://doi.org/10.1109/TCAD.2024.3524333

Ni ZP, Xia J, Zhou XY, et al., 2025b. Design of a wideband symmetric large back-off range Doherty power amplifier based on impedance and phase hybrid optimization. *Front Inform Technol Electron Eng*, 26(1):146-156. https://doi.org/10.1109/FITEE.2400066

Ni ZP, Xia J, Zhou XY, et al., 2025c. Optimization design of ultra-wideband PA with fragment-type structure using load impedance overlap and geometrical constraint. *IEEE Trans Microw Theory Tech*, 73(8):4866-4879. https://doi.org/10.1109/TMTT.2024.3524417

Pang JZ, He SB, Huang CY, et al., 2015. A post-matching Doherty power amplifier employing low-order impedance inverters for broadband applications. *IEEE Trans Microw Theory Tech*, 63(12):4061-4071. https://doi.org/10.1109/TMTT.2015.2495201

Sun JX, Lin F, Li B, et al., 2023. Continuous class-J/F^{-1} mode asymmetrical Doherty power amplifier with extended bandwidth and enhanced efficiency. *IEEE Trans Microw Theory Tech*, 71(11):4814-4825. https://doi.org/10.1109/TMTT.2023.3275177

Xia J, Yang M, Guo Y, et al., 2016. A broadband high-efficiency Doherty power amplifier with integrated compensating reactance. *IEEE Trans Microw Theory Tech*, 64(7):2014-2024. https://doi.org/10.1109/TMTT.2016.2574861

Xiao F, Dai ZJ, Pang JZ, et al., 2021. A Doherty power amplifier with extended back-off by using non-infinite peaking impedance and complex combining load. IEEE MTT-S Int Microwave Workshop Series on Advanced Materials and Processes for RF and THz Applications, p.182-184. https://doi.org/10.1109/IMWS-AMP53428.2021.9643873

Xiao ZH, You F, Shen C, et al., 2023. A Doherty power amplifier based on AM-AM/PM cancellation combining network synthesized by back-off complex load impedance. *IEEE Microw Wirel Technol Lett*, 33(9):1333-1336. https://doi.org/10.1109/LMWT.2023.3292571

Yang ZX, Yao Y, Li MY, et al., 2019. Bandwidth extension of Doherty power amplifier using complex combining load with noninfinity peaking impedance. *IEEE Trans Microw Theory Tech*, 67(2):765-777. https://doi.org/10.1109/TMTT.2018.2884415

Zhang H, Xia J, Zhou X, et al., 2024. Optimization design of irregular broadband Doherty power amplifier based on 3-port output combining network. IEEE MTT-S Int Wireless Symp, p.1-3. https://doi.org/10.1109/IWS61525.2024.10713727

Zhang H, Xia J, Ni ZP, et al., 2025. Optimization design of output combining network using irregular structure for broadband DPA. *IEEE Microw Wirel Technol Lett*, 35(4):480-483. https://doi.org/10.1109/LMWT.2025.3534192

Zhang Y, Pang JZ, Gao RB, et al., 2025a. Dual-wideband three-stage Doherty power amplifier using reciprocal bias configuration. *IEEE Trans Microw Theory Tech*, 73(9):6209-6220. https://doi.org/10.1109/TMTT.2025.3551738

Zhang Y, Gao RB, Liu S, et al., 2025b. One-dimensional reconfigurable three-stage Doherty power amplifier with load mismatch resilience. *Front Inform Technol Electron Eng*, 26(6):1002-1016. https://doi.org/10.1631/FITEE.2400913

Zhang ZW, Fusco V, Cheng ZQ, et al., 2022. A broadband Doherty-like power amplifier with large power back-off range. *IEEE Trans Circ Syst II Expr Briefs*, 69(6):2722-2726. https://doi.org/10.1109/TCSII.2022.3151239

Zhao YL, Li X, Gai C, et al., 2021. Theory and design methodology for reverse-modulated dual-branch power amplifiers applied to a 4G/5G broadband GaN MMIC PA design. *IEEE Trans Microw Theory Tech*, 69(6):3120-3131. https://doi.org/10.1109/TMTT.2021.3073374

Zhou XY, Zheng SY, Chan WS, et al., 2017. Broadband efficiency-enhanced mutually coupled harmonic postmatching Doherty power amplifier. *IEEE Trans Circ Syst I Regul Pap*, 64(7):1758-1771. https://doi.org/10.1109/TCSI.2017.2658689

Zhou XY, Chan WS, Feng W, et al., 2022. Broadband Doherty power amplifier based on coupled phase compensation network. *IEEE Trans Microw Theory Tech*, 70(1):210-221. https://doi.org/10.1109/TMTT.2021.3057628